ADVANCED MATERIALS TECHNOLOGIES
www.advmattechnol.de

Stretchable and Photothermal MXene/PAA Hydrogel in Strain Sensor for Wearable Human-Machine Interaction Electronics

Yan Bai, Yuyuan Lu, Shuaihang Bi, Weikang Wang, Feifei Lin, Fu Zhu, Pin Yang, Ning Ding, Shujuan Liu, Weiwei Zhao, Ning Liu,* and Qiang Zhao**

Wearable human-machine interaction (HMI) is an advanced technology that realizes operations, collaborations, and interactions between human and machines in a co-located or coordinated way. As the core component of wearable HMI electronics, the flexible sensor is desirable to be intelligent, accurate, collaborative, and multifunctional for the feedback control. Here, the multifunctional MXene/polyacrylic acid (PAA) hydrogel is prepared by radical polymerization. As a flexible strain sensor, it exhibits high sensitivity (gauge factor ≈4.94), wide detection range (0–1081%) and stable signal output for 500 cycles. It can also monitor human movement and operate manipulator in real time, exhibiting great potential in wearable artificial intelligence and HMI. Furthermore, the MXene/PAA hydrogel shows photothermal conversion performance with controllable surface temperature regulation ability (RT ≈67 °C) under near-infrared radiation. This work sheds a new light to develop the collaborative and multifunction wearable HMI electronics through integrating the flexible sensor with personal thermal management system.

1. Introduction

As a bridge between human and scientific information, wearable human-machine interactions (HMI) electronics are an inevitable future trend in wise information technology of medicine,[1,2] smart home,[3,4] robot technology,[5,6] and other advanced fields.[7,8] The basic flexible sensor requires to obtain the feedback signal from the human body, and continuously provides the accurate and real-time external information for machine.[9] The materials of flexible sensor should comply with the following criteria: i) excellent flexibility to match human tissue, ii) high and stable conductivity to rapidly and reliably respond the signals, iii) tight adhesion to human body surface, iv) safety and nontoxic to contact with the human body. Hydrogel is a kind of highly hydrophilic 3D network gel, which are like human tissues in structure and composition.[10] For example, our research group has prepared a 3D porous cellulose hydrogel to realize a highly sensitive flexible strain sensor.[11] Tao et al. fabricated a micropyramid-patterned double-network ionic organ hydrogels for flexible sensor to detect subtle pressure changes.[12] They are desirable to satisfy the requirement of flexible sensor by the unique properties including flexibility, extreme precision, high durability, and skin-friendliness by the adjusted structure and components. At present, it is limited to the development of a single function in wearable HMI electronics. However, it is still a challenge to develop multifunction hydrogel with excellent properties for high-precision flexible strain sensor to achieve precise control in wearable HMI electronics.

The personal thermal management (PTM) technology provides specific temperature control and health monitoring for various novel interactive ways of wearable HMI electronics, and effectively improve practicality and user experience.[13,14] As one of the representative categories, photothermal conversion technology converts light energy into thermal energy by reflection and absorption, which conforms to the concept of energy saving and has been applied in PTM technology.[15,16] Nowadays, flexible hydrogels with excellent photothermal property have been obtained by introducing photothermal conversion agents (i.e., carbon nanomaterials,[17] organic materials,[18] metal materials,[19] and semiconductor materials[20]) into the matrix. As a new type of 2D transition metal carbides and nitrides, MXene has exhibited prominent photothermal conversion performance due to the profits from high light absorption and the localized surface plasmon resonance (LSPR) effect.[21,22] Accordingly, MXene hydrogel is one of the suitable candidates for flexible photothermal materials, which can be used in the

Y. Bai, Y. Lu, S. Bi, W. Wang, F. Lin, P. Yang, N. Ding, S. Liu, W. Zhao, Q. Zhao
State Key Laboratory of Organic Electronics and Information Displays & Jiangsu Key Laboratory for Biosensors
Institute of Advanced Materials (IAM)
Nanjing University of Posts & Telecommunications
9 Wenyuan Road, Nanjing 210023, P. R. China
E-mail: iamwwzhao@njupt.edu.cn; iamqzhao@njupt.edu.cn

F. Zhu, N. Liu, Q. Zhao
College of Electronic and Optical Engineering & College of Flexible Electronics (Future Technology)
Nanjing University of Posts & Telecommunications (NUPT)
9 Wenyuan, Nanjing 210023, P. R. China
E-mail: liuning0127@njupt.edu.cn

The ORCID identification number(s) for the author(s) of this article can be found under https://doi.org/10.1002/admt.202201767.

DOI: 10.1002/admt.202201767

field of thermal physiotherapy,[23] temperature sensing,[24] and heat preservation.[25] For example, Zhao et al. have combined MXene with N-isopropylacrylamide to prepare an intelligent hydrogel for temperature/pH dual response.[24] He et al. fabricated a polysaccharide/MXene hydrogel sensor with photothermal property for in vitro photothermal conversion.[26] However, the potential integration of photothermal conversion and flexible sensor to achieve excellent temperature control and physiological monitoring is still rarely reported. Therefore, it is a challenge to develop hydrogel materials that combine the functions of PTM and flexible sensor to provide a multifunctional platform with portable therapeutic instruments and electronic manufactures in the fields of HMI.

Herein, we demonstrate the free-radical polymerized MXene/polyacrylic acid (PAA) hydrogel with high strain sensitivity and adjustable photothermal conversion performance for the wearable HMI electronics. The dynamic hydrogen bonding enables to achieve fast self-healing (≈1.3 s), and strong adhesion on different hydrophilic and hydrophobic substrates. Meanwhile, the wonderful biocompatibility lays the foundation for flexible environmentally-friendly wearable devices. The outstanding photothermal conversion property endows MXene/PAA hydrogel suitable for PTM. Furthermore, MXene/PAA hydrogel based flexible strain sensor can not only quickly sense human motion detection and accurately capture small strain physiological activity such as frown, smile and throat, but also can be controlled remotely to monitor intelligent robots. As a proof of concept, this work inspires the potential application of multifunctional MXene/PAA hydrogel in the field of movement monitoring, remote control, intelligent medicine, thermal physiotherapy, temperature sensing, and heat preservation in wearable HMI electronics.

2. Results and Discussion

2.1. Preparation and Characterization of MXene/PAA Hydrogel

The schematic illustration of the MXene/PAA hydrogel is demonstrated in **Figure 1**a. First, ultrathin 2D MXene nanosheets are obtained by ultrasonic stripping of multilayered MXene (Figure S1, Supporting Information). Then, the acrylic acid (AA) monomer and MXene nanosheets are mixed with the solution of ammonium persulfate (APS) and N,N'-methylenebisacrylamide (MBAA).[27] PAA is synthesized by free radical polymerization from AA monomer under the aid of MBAA as a chemical crosslinking agent and APS as an initiator.[28] Meanwhile, MXene nanosheets with rich surface functional groups (i.e., -O, -F, and -OH) exist hydrogen bond interaction with the carboxyl groups on the PAA. Finally, MXene/PAA hydrogel is generated at 60 °C for 4 h.

To better understand the formation mechanism, MXene/PAA hydrogels are systematically characterized. In comparison with the pure PAA hydrogel, MXene/PAA hydrogel has an increased pore density (Figure 1b; Figure S2, Supporting Information). It is ascribed that the rich hydrogen bond interactions between MXene and PAA not only embed MXene nanosheets into the polymer network structure but also increase network density.[29] MXene/PAA hydrogel has the (002) characteristic peak at $2\theta = 6.37°$, which has a negative peak shift from

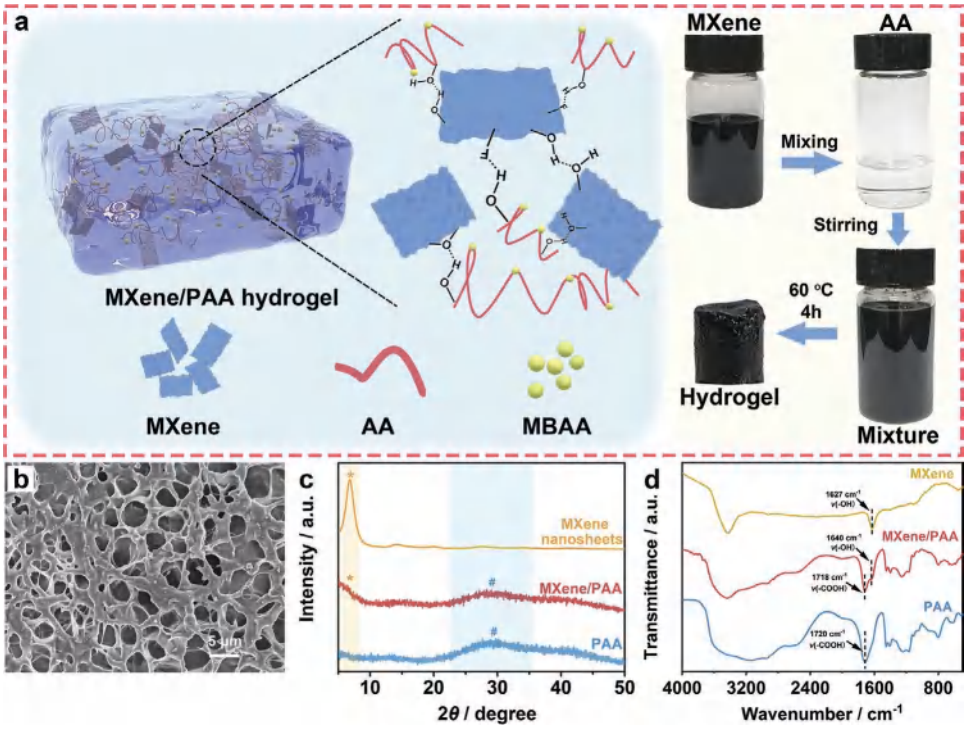

Figure 1. Design and characterization of MXene/PAA hydrogel. a) Schematic illustration of the synthesis route and b) SEM image of MXene/PAA hydrogel. c) XRD patterns and d) FT-IR spectra of MXene nanosheets, PAA hydrogel and MXene/PAA hydrogel.

2θ = 6.8° for pure MXene nanosheets (Figure 1c). It demonstrates that *d*-spacing of MXene increases from 1.3 nm for pristine MXene to 1.386 nm for MXene/PAA, which is attributed to the insertion of PAA chains between MXene nanosheets.[30] FT-IR spectra are performed to provide more detailed information for elucidating the cross-linking structure (Figure 1d). From the spectrum of PAA hydrogel, the peak at 1720 cm^{-1} can be assigned to the -COOH group. Compared with PAA hydrogel, a new characteristic peak appears at 1640 cm^{-1} for MXene/PAA hydrogel, which is assigned to -OH group of MXene. Meanwhile, the -COOH characteristic peak exhibits a slight shift due to the formation of hydrogen bonds.[31] As a result, MXene/PAA hydrogel with 3D porous structure is prepared successfully by simple free radical polymerization.

2.2. Performance Investigation of MXene/PAA Hydrogel

In order to explore the possibility of applying MXene/PAA hydrogel for wearable HMI electronics, the unique property including mechanical property, conductivity, self-healing, adhesion, biocompatibility are systematically studied. First, the mechanical property of MXene/PAA hydrogel is explored under different deformations. It can quickly return to the initial state after twisting, compression and stretching, presenting excellent mechanical resilience (**Figure 2**a; Figure S3, Supporting Information). At the same time, the hydrogel effectively stretches in a knot, exhibiting the strong toughness to accommodate local stress concentration (Figure 2b). Furthermore, there is no crack or even a scratch on the surface after being pressed by a sharp scissor, proving great puncture resistance (Figure 2c). The hydrogel can load 200 g weight without breakage, revealing strong mechanical strength (Figure 2d). It also exhibits good shapeability, and lays a foundation for flexible electronics (Figure 2e).

To investigate the influence of MXene content on the property, MXene/PAA hydrogels with different mass ratio of MXene (i.e., 0%, 1%, 2%, 3%, 4%, and 5%) are prepared (Table S1, Supporting Information). Firstly, the effect of MXene addition on tensile property is studied (Figure 2f; Table S2, Supporting Information). When the mass ratio of MXene increases from 0 to 4%, the strain increases from 679% to 1081% and the corresponding stress raises from 25.55 to 101.00 kPa, proving the greatly increased ductility and toughness. It is attributed to the hydrogen bond interaction between MXene and PAA.[32] When the mass ratio of MXene further increases to 5%, the stress increases to 120.86 kPa and the strain decreases to 1007%. The excessive MXene nanosheets will lead to self-accumulation and agglomeration, which will make the hydrogel network uneven and the movement resistance increases.[33] Interestingly, the Young's modulus increases from 3.76 to 12 kPa with the mass ratio of MXene/PAA from 0 to 5% (Figure S4, Supporting Information), indicating that MXene nanosheets increase the cross-linking degree of the 3D network to effectively enhance the rigidity. In terms of the flexibility and robustness, the MXene/PAA hydrogel with an optimal MXene proportion of 4 wt.% exhibits the maximum tensile fracture length of 1081%, which is superior to the reported hydrogels (Table S3, Supporting Information).

Furthermore, we also evaluate the influence of different mass ratio of MXene on the conductivity (Figure 2g; Table S2,

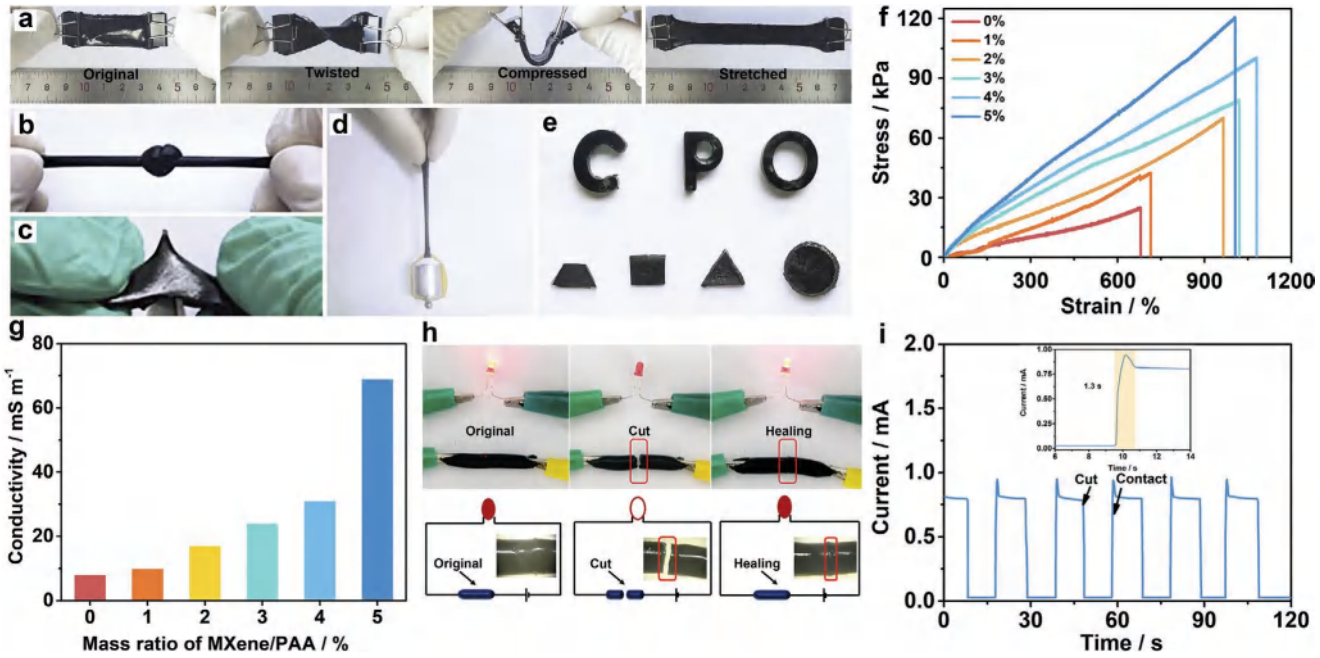

Figure 2. Performance investigation of the hydrogel. Photographs of flexible MXene/PAA hydrogel in different states. Original, twisted, compressed and stretched states a), stretching after making a knot b), bearing the sharp pressure of a scissor c), lifting 200 g weight d), and shapeability e). Stress–strain curves f) and conductivity g) of MXene/PAA hydrogel with different mass ratio of MXene. h) Photographs of LED brightness change at different MXene/PAA hydrogel states (i.e., original, cut and healing) and corresponding schematic diagrams of circuit diagram. i) Current change curves of MXene/PAA hydrogel before and after self-healing.

Supporting Information). With the increases of MXene mass ratio, the conductivity of MXene/PAA hydrogel gradually increases from 8 to 69 mS m^{-1}, which is better than the reported literatures (Table S4, Supporting Information). The main reason is that the higher proportion of MXene enhances the crosslinking density of 3D MXene/PAA hydrogel network and generates more conductive pathways.[34,35] Based on the excellent mechanical and electrical property, MXene/PAA hydrogel with a mass ratio of 4% are selected for performance measurement.

Dynamic hydrogen bonding interactions endow MXene/PAA hydrogel with eminent self-healing. To observe the experimental phenomenon intuitively, the conductive MXene/PAA hydrogel is used as a wire to light up light-emitting diode (LED) at a voltage of 1.5 V (Figure 2h). Upon the hydrogel is cut into two parts, the circuit is disconnected, causing the LED to go out. After repairing the broken hydrogel, LED can be lit up again. At the same time, it is observed by the optical microscope that the healed MXene/PAA hydrogel has no obvious wound compared with the original hydrogel, displaying the efficient self-healing. A real-time current measurment system is adopted to monitor the current variation and repeatability of MXene/PAA hydrogel undergoing the self-healing process (Figure 2i). Similar to the experimental phenomenon, the current rapidly drops to 0 mA when the hydrogel is cut in half, indicating no current passes through the open circuit. Subsequently, after bonding the fractured hydrogels together for 1.3 s, the current almost returns to the initial state, which is better than other self-healing hydrogels.[36,37] The cutting-healing process is completely repeatable for five times with the self-healing efficiency of 99%. It proves that MXene/PAA hydrogel possesses the excellent self-healing ability, which renders it advantageous application in flexible wearable self-healing epidermal sensors. For wearable HMI electronics, the self-healing ability of hydrogel can prolong service life, improve durability, practicability, reliability, and reduce economic costs.[38,39]

Most hydrogels require additional adhesives to adhere to skin or clothing, resulting in poor flexibility and greatly hindering their applications in wearable HMI electronics. The MXene/PAA hydrogel with excellent adhesion can adhere to hydrophilic and hydrophobic substrates including plastic, metal, skin, and glass (**Figure 3**a). Even if the finger is bent to 90°, the hydrogel can firmly adhere to the skin, showing a tight adhesion. Concretely, the adhesion and repeatability of MXene/PAA hydrogel on different substrates (i.e., plastic, metal, skin, and glass) are measured. The adhesion strength is maintained at ≈13.71 kPa for plastic, 18.01 kPa for metal (copper plate), 18.76 kPa for skin, and 36.58 kPa for glass after three cycles (Figure 3b), which is similar to the previously reported hydrogel materials.[40,41] There is almost no significant loss in adhesion strength, indicating an excellent adhesive repeatability. It is ascribed that the electrostatic interaction between the functional groups (e.g., carboxyl groups in PAA matrix and groups (i.e., -OH, -F, = O) of MXene nanosheets) with the different surfaces.[42,43] Interestingly, hydrogels can be stripped from different substrates without any residues (Figure S5; Video S1, Supporting Information), indicating the suitable adhesion can not cause the damage of hydrogel structure and the contamination of substrate. The adhesiveness is vital for the interface connection of wearable HMI electronics, it can effectively reduce the decline of signal quality caused by the gap between the contact surface, and can also achieve stable adhesion to the intrinsic bending of materials.[44,45]

The direct adhesion of hydrogel to human body without harm is one of the prerequisites for wearable HMI electronics.

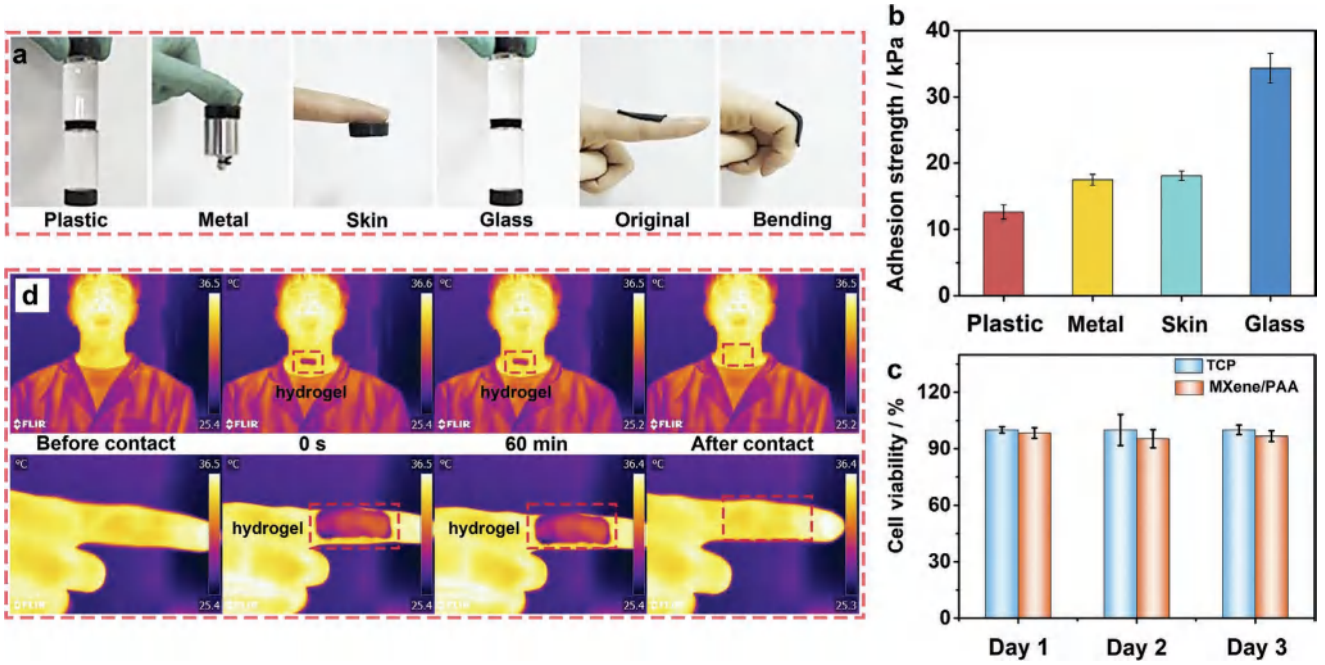

Figure 3. Performance analysis of the MXene/PAA hydrogel. a) Photographs illustrate the adhesiveness to diverse surfaces. b) Adhesive strength to various substrates. c) Cell viability of cells cultured with TCP and MXene/PAA hydrogel. d) IR thermal images of the neck and finger before and after contacting the MXene/PAA hydrogels for 60 min.

We co-culture MXene/PAA hydrogel extract with L02 cells for 3 days to verify the biocompatibility. Compared with tissue culture plate (TCP), the cell viability does not significantly decrease, and remains above 95% (Figure 3c). Furthermore, the LIVE/DEAD assay is carried out to observe the viability of cells intuitively. The fluorescence images reveal that the survival cells (green staining) are evenly distributed in each group, and the cell density increases significantly during the culture process, suggesting that the hydrogel is non-toxic and processes excellent biocompatibility (Figure S6, Supporting Information). Interestingly, the adhesion of MXene/PAA hydrogel to the throat and finger displays no allergy or significant temperature change after 60 min (Figure 3d). It indicates that the attached hydrogels can not only safely contact with the human body, but also exhibits great heat dissipation performance, exhibiting a wide application prospect in wearable flexible devices.

2.3. Photothermal Conversion Performance of MXene/PAA Hydrogel

Hydrogel based strain sensor can be applied to PTM depending on the brilliant photothermal conversion performance, which enables the versatile functionality in wearable HMI electronics,[46] disease therapies[47] and so on. The photothermal property of MXene/PAA hydrogel is measured under NIR light radiation (808 nm) with different power densities (i.e. 200, 300, 400, and 500 mW cm^{-2}) for 300 s (**Figure 4**a,b; Figure S7a, Supporting Information). The surface temperature of hydrogel can reach up to 35.5, 42.5, 53, and 67 °C at the consecutively increased irradiation intensity, respectively. It indicates the controllable photothermal performance of MXene/PAA hydrogel, which is also superior to the reported materials (Table S5, Supporting Information). Meanwhile, the temperature no longer rises after turning off the light, showing the outstanding photothermal conversion sensitivity. In comparison, the temperature of the PAA hydrogel shows little increase in the absence of MXene nanosheets (Figure S7b, Supporting Information). The photothermal conversion mechanism of MXene/PAA hydrogel derives from the generation of photothermal electrons induced by the LSPR effect of MXene (Figure 4c).[48] Once the NIR light is turned off, it gradually returns to the initial temperature by thermal release. To further explore the photothermal stability of MXene/PAA hydrogel, the temperature variation under light on/off measurement is recorded under 808 nm NIR irradiation of 300 mW cm^{-2} for 5 cycles (Figure 4d). The peak temperature and response time are well maintained without any deterioration upon the cycling, exhibiting the excellent reproducibility of photothermal conversion. It is well known that the conductivity is proportional to temperature within limits.[49] The response current of MXene/PAA hydrogel increases with the increase of power density, and the signal output of each cycle is stable (Figure 4e). In other words, due to the excellent photothermal conversion performance, MXene/PAA hydrogel leads to the increased temperature under NIR irradiation, which accelerates the carrier migration and produces a sensitive current response.[50] Furthermore, to verify the feasibility of MXene/PAA hydrogel as a wearable heater, the hydrogel is attached to human skin (Figure 4f). The initial temperature of hand and hydrogel are 35.2 °C and

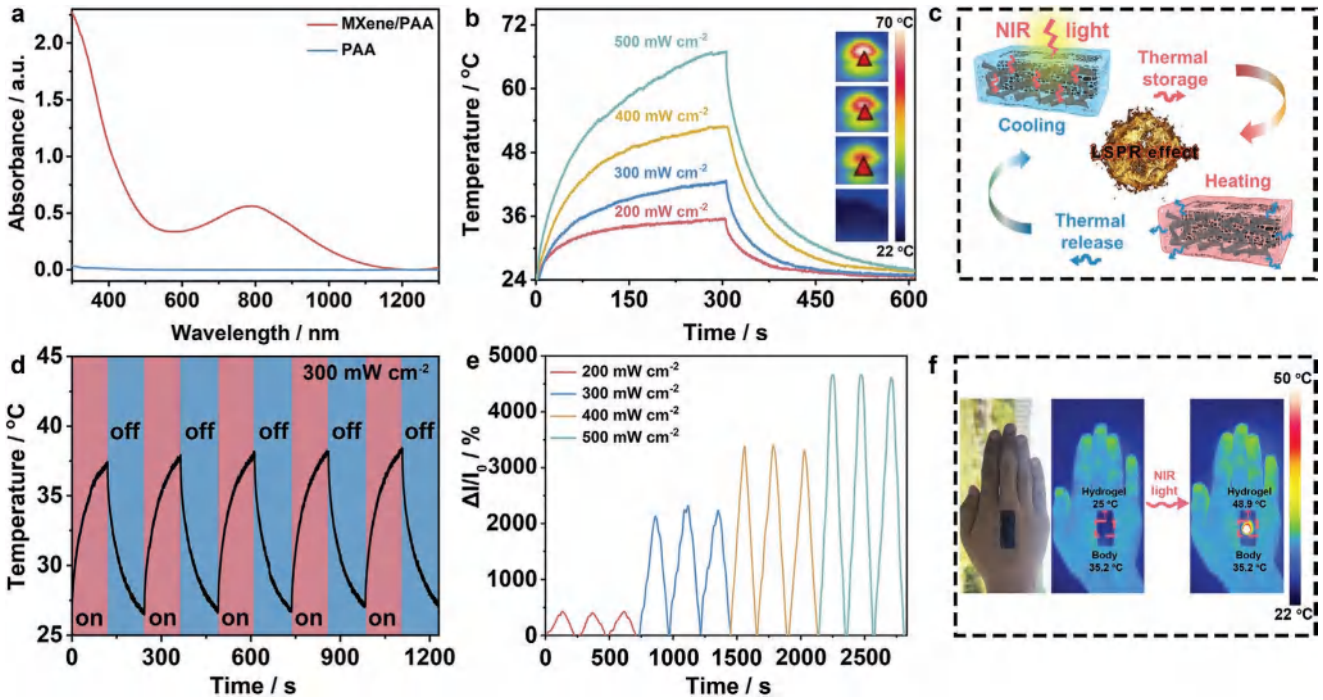

Figure 4. Photothermal conversion performance of MXene/PAA hydrogel. a) UV–vis-NIR spectra of PAA hydrogel and MXene/PAA hydrogel. b) Temperature-time curves and NIR images of MXene/PAA hydrogel under NIR irradiation with different power densities. c) The photothermal conversion mechanism of MXene/PAA hydrogel. d) Cyclic stability of MXene/PAA hydrogel at 300 mW cm^{-2} for 5 on/off cycles. e) The current response under different power densities. f) Photographs and IR thermal images of hydrogel on the hand before and after irradiation.

25 °C, respectively. After irradiation for 150 s at 400 mW cm^{-2}, the temperature rises to 48.9 °C, while the temperature of other parts well maintains. In combination with previous properties, MXene/PAA hydrogel plays a potential role for PTM in wearable HMI electronics, health care, and other fields.

2.4. Sensing Performance of Wearable Strain Sensor

Based on the excellent conductivity, stretchability, self-healing, adhesion, biocompatibility of MXene/PAA hydrogel, it can be used to prepare flexible strain sensor for wearable HMI electronics. To evaluate the sensing performance, the MXene/PAA hydrogel is covered with two pieces of copper foils for electrochemical measurement. First, the tensile sensitivity of MXene/PAA hydrogel is tested. The gauge factor (GF) of the strain sensor is 1.69, 3.23, and 4.94 in the strain range of 0 – 250%, 250 – 625%, and 625 – 1081%, respectively (**Figure 5**a). The MXene/PAA hydrogel exhibits a higher sensitivity than the PAA hydrogel and the previously reported hydrogel materials (Figure 5b).[51–60] The increased resistance under different strain ranges is attributed to the resistance variation of the MXene-based 3D conductive network including island resistance, gap resistance, and contact resistance.[61,62] With the significant decline of conductive paths, the tunneling resistance sharply rises with the ascending tension and achieves a highly enhanced GF. It is indicated that MXene as a conductive filler can effectively improve the sensitivity of MXene/PAA hydrogel sensor. Figure 5c presents the sensing response of MXene/PAA hydrogels under the tensile deformation (i.e., 30%, 60%, and 90%). The relative resistance change of MXene/PAA hydrogel increases with the applied strain, and exhibits stable repeatability in 5 consecutive cycles. It proves that the hydrogel can be used as a strain sensor to monitor different tensile strains, and has good reliability. Meanwhile, the MXene/PAA hydrogel strain sensor can maintain stable signal output after 500 cycles for 30% strain (Figure 5d). These results show that the MXene/PAA hydrogel sensor processes high sensitivity, excellent

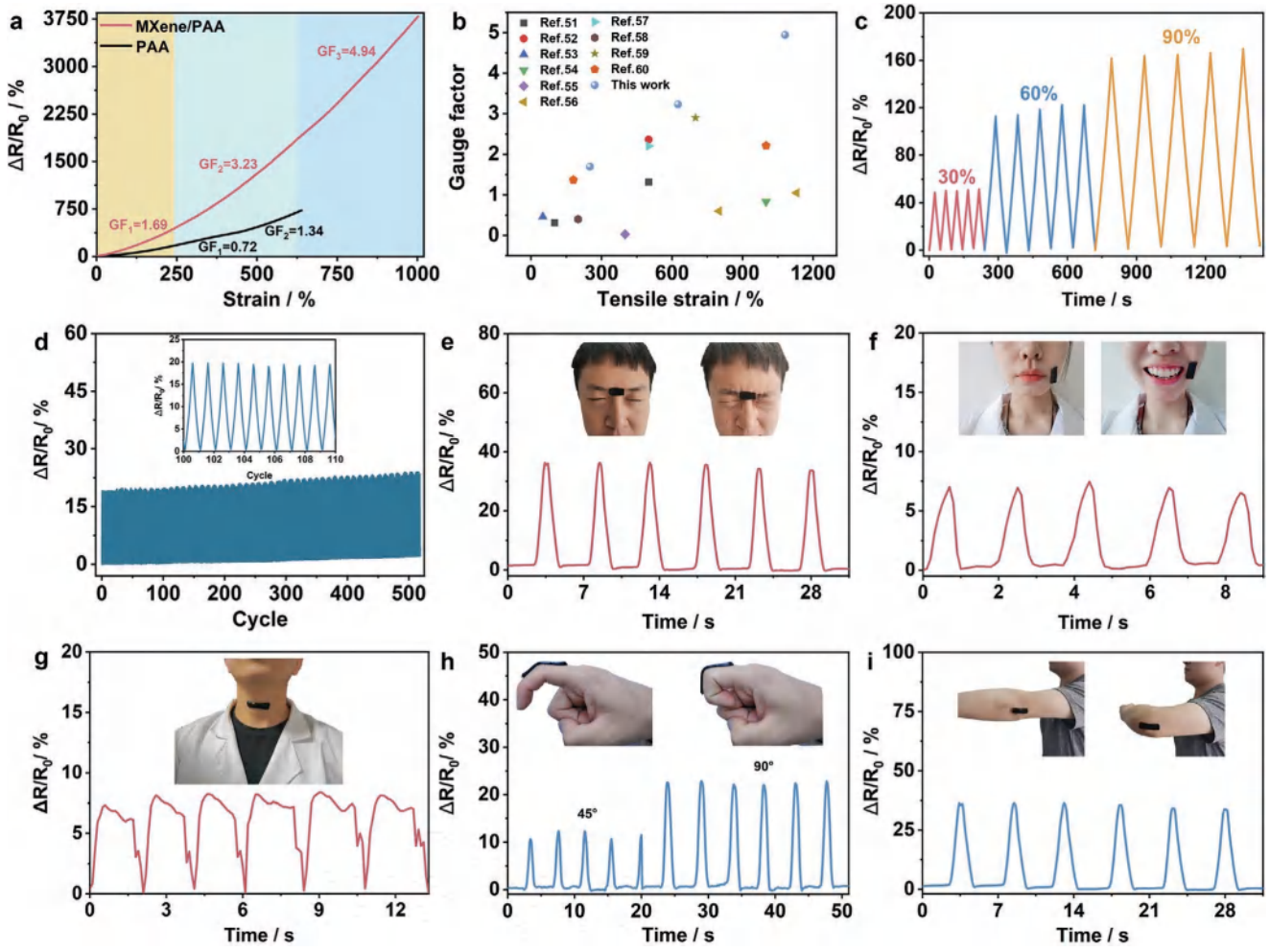

Figure 5. Sensing performance of MXene/PAA hydrogel. a) Relative resistance-tensile strain curves of MXene/PAA hydrogel and PAA hydrogel. b) Comparison of tensile GF between MXene/PAA hydrogel and other hydrogel materials published in the literature. c) Relative resistance variation under different strains (i.e., 30%, 60%, and 90%). (d) Relative resistance stability of the stain sensor during 5000 s at the strain of 30%. Applications of MXene/PAA hydrogel sensors. Real-time recording of the relative resistance changes generated by various human activities of the eyebrow e), mouth f), throat g), finger h), and elbow i).

stability, repeatability, and has great application potential in the field of wearable HMI electronics as a flexible strain sensor.

The MXene/PAA hydrogel can be assembled and attached to the human body as a non-irritating wearable strain sensor for human biomonitoring (Figure 5e–i; Video S2, Supporting Information). The sensor is applied to identify various subtle and large-scale human motions. By attaching the sensor to eyebrows, mouth corners and throat, the sensor can sense the signal changes clearly caused by small movements such as frowning, smiling, and swallowing (Figure 5e–g). It is indicated that the MXene/PAA hydrogel sensor can accurately detect tiny human movements, and exhibit the potential for facial recognition. Furthermore, when the sensor is attached to the finger and elbow (Figure 5h,i), the relative resistance changes under the a certain of bending angles, and the signal output is stable and repeatable. It shows the application potential for MXene/PAA hydrogel to be widely used in motion detection and intelligent medical fields.

2.5. Application of MXene/PAA Hydrogel Strain Sensor

The MXene/PAA hydrogel is expected to realize the control of the manipulator for the application potentials in wearable HMI electronics. In order to realize the accurate control of the motion mode of the manipulator, 16-bit high precision analog-to-digital conversion chip is used to complete the conversion of analog electrical signals to digital signals of five fingers, and complete wireless transmission and control through Bluetooth module, which ensures the high synchronization of human movement and manipulator movement in terms of performance. After calculation, the synchronization rate is as high as 99%, and the control delay is <3 ms. The signal acquisition circuits and controlling circuits are constructed in **Figure 6**a. The resistance change of the sensor is collected and then converted into an output voltage signal, which is further transmitted to the microcontrol unit. Subsequently, a microprocessor controls the motor to bend the fingers of robot (Figure 6b). In this study, a real-time calibration correction matching technique is specially designed. It can ensure that the relative electrical signals are generated during each stretching, and the reset electrical signals will not exceed the working range. The real-time linear mapping technology combines high-precision modules sampling and high-speed Bluetooth short-range transmission characteristics to achieve near 0 delay linear mimicry motion,[63] which is different from the existing control methods.[64] The experimental results show that MXene/PAA hydrogel can not only control the manipulator to complete a simple opening and closing state, but also feel subtle deformation and achieve continuous hovering, following and other movements (Figure 6c; Video S3, Supporting Information). The high- precision MXene/PAA hydrogel based strain sensor can achieve the precise control of wearable HMI electronics, which provides a technical feasibility demonstration for the follow-up industrial application. Comprehensively, MXene/PAA hydrogel can be used in diversified forms for wearable HMI electronics, such as movement monitoring, remote control, intelligent medicine, thermal physiotherapy, temperature sensing, and heat preservation (Figure 6d).

3. Conclusion

In conclusion, we have explored the free-radical polymerized MXene/PAA hydrogel for the multifunctional applications in wearable HMI electronics. The photothermal conversion performance of MXene/PAA hydrogel endows it direct applications in PTM. The corresponding flexible sensor exhibits the excellent advantages of high sensitivity, wide detection range, and cyclic stability. It can monitor the human motion signal in real time and remotely control the manipulator, showing the perception feedback of intelligent robot in HMI. The combination of flexible sensor and PTM is beneficial to realize the functions of health monitoring and temperature control, which further expands the scope of application and enhances the practicality. This work paves an avenue for the development of flexible wearable HMI electronics toward multifunction, high precision, durability, and green environmental protection in the future.

4. Experimental Section

Materials: Ti_3AlC_2 was commercially purchased from Jilin 11 Technology Co., Ltd. Hydrochloric acid (HCl, 37%) and ammonium persulfate (APS) were obtained from Shanghai Sinopharm Group Co., Ltd. Lithium fluoride (LiF) was purchased from Shanghai Aladdin Biochemical Technology Co., Ltd. Acrylic acid (AA, 99%) was purchased from Energy Chemical Technology Co., Ltd. N,N'-methylenebisacrylamide (MBAA) was purchased from Shanghai Macklin Biochemical Co., Ltd. Mdium DMEM (BR), thiazole blue (BR), phosphate buffer (BR), and LIVE/DEAD cell staining Kit (BR) were commercially purchased from Jiangsu Keygen Biotech Co., Ltd. All the above-mentioned chemicals were used without any further purification.

Characterizations: The morphology and structure were observed by scanning electron microscopy (SEM, Hitachi S-4800). The morphology of MXene nanosheets was measured by transmission electron microscope (TEM, Hitachi HT7700). The X-ray diffraction (XRD) patterns were obtained by X-ray diffractometer (Bruker AXS D8 Advance) using Cu $K\alpha$ radiation (λ = 1.5418 Å). Chemical compositions of samples were confirmed with Fourier transform infrared spectra (FT-IR, Perkin Elmer, PE-Spectrum Two). To carry out the characterization test, the hydrogel samples were freeze-dried for 3 days by freeze drying machine (BILON FD-1A-50).

Tensile tests of hydrogel were performed on a tensile testing tester (INSTRON 3365) with a loading rate of 40 mm min^{-1}. The tensile stress (σ) was calculated as $\sigma = F/S$, where F was the tensile load (N) and S was the original cross section area (m^2). The tension strain (ε) was defined as $(L–L_0)/L_0 \times 100\%$, where L_0 was the initial length of hydrogel (mm) and L was the broken length of hydrogel (mm).[11] The adhesive strength of MXene/PAA hydrogels was tested via stress-strain test at a tensile rate of 5 mm min^{-1}. Electrochemical impedance spectroscopy (EIS) was used to characterize the conductivity of rectangular hydrogel (20 mm × 10 mm × 2 mm) by the electrochemical workstation (CHI 660E). The conductivity was calculated as L/RS, where R was the resistance (Ω), L and S were the length (m) and cross-sectional area (m^2), respectively.[65] The biocompatibility investigation of the MXene/PAA hydrogel was evaluated.[66] After the growth of adherent cells, the culture medium soaked in hydrogel was added and incubated in the incubator for different periods of time. Then calcein-AM and propidium iodide (PI) were added to label cells. Calcein-am could label living cells, and PI could label dead cells. The sensitivity of a strain sensor was defined as a gauge factor (GF) and calculated by the formula: $GF = (\Delta R/R_0)/\varepsilon$, where $\Delta R = R–R_0$, R_0 and R were the raw resistance and the resistance under deformation respectively, and ε was the applied strain.[67] The 488 nm laser was used to collect fluorescence signals

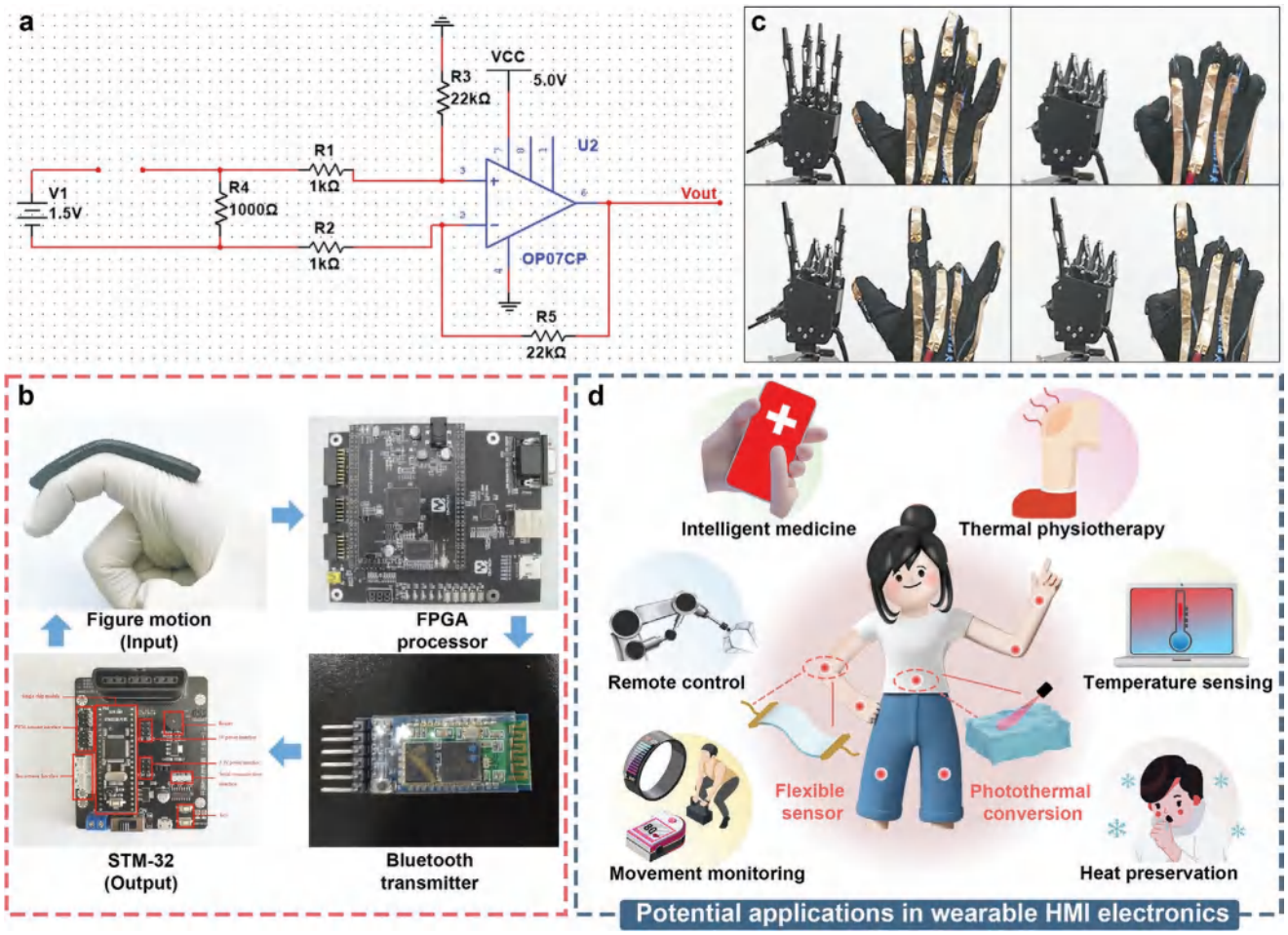

Figure 6. Application of MXene/PAA hydrogel in wearable HMI electronics. a) The electronic circuit of MXene/PAA strain sensor on the application of finger motions detection. b) Illustration of the instant controlling process of robot hand. c) Photographs of MXene/PAA hydrogel sensors control manipulator in real time. d) Schematic diagram of the potential applications in the wearable HMI electronics.

in the 500 – 550 nm and 600 – 650 nm bands, respectively. The cells were inoculated on the tissue culture plate (TCP) without hydrogel as the control group. The ultraviolet-visible-near-infrared (UV–vis-NIR) spectra were recorded using a Shimadzu UV-3600 spectrophotometer at the scanning range of 300 – 1300 nm. The temperature change of the sample was captured in real time by Infrared thermal imager (FLIR E40).

Synthesis of MXene Nanosheets: The MXene nanosheets were prepared by selectively etching Al layer from Ti_3AlC_2 bulks, referring to the previously reported work.[68] First, LiF (1 g) was added to HCl (9 M, 20 mL) and stirred for 20 min. Then, the Ti_3AlC_2 blocks (1 g) were slowly added and heated at 60 °C for 24 h. Afterward, the products were washed several times with deionized water until the pH was above 6. Next, the samples were dried under vacuum for 12 h. To get the MXene nanosheets, multilayer MXene was dispersed in deionized water under Ar and sonicated for 1 h. Finally, the dispersion was centrifuged at 3500 rpm for 1 h, and the supernatant was collected for the further application.

Synthesis of MXene/PAA Hydrogel: First, APS (25 mg) and MBAA (2 mg) were dissolved in deionized water (3 mL) to prepare APS and MBAA mixture solution. Then, AA (2.5 mL) was added to the above suspension, and the suspension was uniformly stirred in the ice-water bath. Next, MXene nanosheets were added according to the different mass ratio of MXene/PAA. Finally, the hydrogel was formed after the reaction for 4 h at 60 °C.

Sensing Test of MXene/PAA Hydrogel: The electrical signal of the pressure sensor was obtained from the amperometry *I–T* curve of the electrochemical workstation (CHI 660E) at the voltage of 1 V. The hydrogel bioelectrode was prepared by attaching MXene/PAA hydrogel to conductive wire. This hydrogel bioelectrode can self-adhere on the skin to record the electric current, which can be used to obtain and record the activity of human.

Photothermal Property of MXene/PAA Hydrogel: The photothermal property was tested by an 808 nm high power NIR light with a 9-mm-radius spot as light source. The hydrogel (15 mm × 15 mm × 2 mm) was directly placed under the near-infrared (NIR) light source at a distance of 5 cm and irradiated at different powers (i.e., 200, 300, 400, and 500 mW cm^{-2}), coupled with the infrared camera to capture the surface temperature in real time. The hydrogel was connected to the electrochemical workstation through the wires to reveal the real time current changes under irradiation.

Supporting Information

Supporting Information is available from the Wiley Online Library or from the author.

Acknowledgements

This work was supported by National Natural Science Foundation of China (62174086 and 62288102), Postgraduate Research &

Practice Innovation Program of Jiangsu Province (KYCX20_0755 and SJCX22_0253).

Conflict of Interest

The authors declare no conflict of interest.

Data Availability Statement

The data that support the findings of this study are available from the corresponding author upon reasonable request.

Keywords

flexible strain sensor, human-machine interaction, MXene/PAA hydrogel, photothermal conversion, personal thermal management system

Received: October 19, 2022
Revised: November 24, 2022
Published online:

[1] P. Rajpurkar, E. Chen, O. Banerjee, E. J. Topol, *Nat. Med.* **2022**, *28*, 31.
[2] Y. Fang, Y. Zou, J. Xu, G. Chen, Y. Zhou, W. Deng, X. Zhao, M. Roustaei, T. K. Hsiai, J. Chen, *Adv. Mater.* **2021**, *33*, 2104178.
[3] X. Zhao, H. Askari, J. Chen, *Joule* **2021**, *5*, 1391.
[4] H. K. Bisoyi, Q. Li, *Chem. Rev.* **2022**, *122*, 4887.
[5] S. Li, Z. Zhao, D. Liu, J. An, Y. Gao, L. Zhou, Y. Li, S. Cui, J. Wang, Z. L. Wang, *Adv. Mater.* **2022**, *34*, 2110363.
[6] M. Kaur, T. H. Kim, W. S. Kim, *Adv. Mater.* **2021**, *33*, 2170148.
[7] Z. Lin, G. Zhang, X. Xiao, C. Au, Y. Zhou, C. Sun, Z. Zhou, R. Yan, E. Fan, S. Si, L. Weng, S. Mathur, J. Yang, J. Chen, *Adv. Funct. Mater.* **2022**, *32*, 2109430.
[8] W. Ding, A. C. Wang, C. Wu, H. Guo, Z. L. Wang, *Adv. Mater. Technol.* **2019**, *4*, 1800487.
[9] W. Heng, S. Solomon, W. Gao, *Adv. Mater.* **2022**, *34*, 2107902.
[10] Y. Zhao, C. Y. Lo, L. Ruan, C. H. Pi, C. Kim, Y. Alsaid, I. Frenkel, R. Rico, T. C. Tsao, X. He, *Sci Robot* **2021**, *6*, eabd5483.
[11] Y. Bai, S. Bi, W. Wang, N. Ding, Y. Lu, M. Jiang, C. Ding, W. Zhao, N. Liu, J. Bian, S. Liu, Q. Zhao, *Soft Mater.* **2022**, *20*, 444.
[12] K. Tao, Z. Chen, J. Yu, H. Zeng, J. Wu, Z. Wu, Q. Jia, P. Li, Y. Fu, H. Chang, W. Yuan, *Adv. Sci.* **2022**, *9*, 2104168.
[13] R. Hu, Y. Liu, S. Shin, S. Huang, X. Ren, W. Shu, J. Cheng, G. Tao, W. Xu, R. Chen, X. Luo, *Adv. Energy Mater.* **2020**, *10*, 1903921.
[14] K. Zhao, J. Cheng, N. Sun, Y. Wang, H. Huang, S. Zhang, W. Niu, *Adv. Mater. Technol.* **2022**, *7*, 2101057.
[15] Q. Lu, X. Wang, *Adv. Sci.* **2022**, *9*, 2104225.
[16] K. Yang, S. Zhao, B. Li, B. Wang, M. Lan, X. Song, *Coord. Chem. Rev.* **2022**, *454*, 214330.
[17] X. Chen, P. Cheng, Z. Tang, X. Xu, H. Gao, G. Wang, *Adv. Sci.* **2021**, *8*, 2001274.
[18] H. Xiang, L. Zhao, L. Yu, H. Chen, C. Wei, Y. Chen, Y. Zhao, *Nat. Commun.* **2021**, *12*, 218.
[19] C. Wang, W. Li, Z. Li, B. Fang, *Renew. Sust. Energy Rev.* **2020**, *134*, 110277.
[20] P. A. Maggard, *Acc. Chem. Res.* **2021**, *54*, 3160.
[21] C. Ma, M. G. Ma, C. Si, X. X. Ji, P. Wan, *Adv. Funct. Mater.* **2021**, *31*, 2009524.
[22] Y. Z. Zhang, J. K. ElDemellawi, Q. Jiang, G. Ge, H. Liang, K. Lee, X. Dong, H. N. Alshareef, *Chem. Soc. Rev.* **2020**, *49*, 7229.
[23] C. Murugan, V. Sharma, R. K. Murugan, G. Malaimegu, A. Sundaramurthy, *J. Controlled Release* **2019**, *299*, 1.
[24] J. Zhao, Y. Li, H. Zhu, G. Li, L. Kang, J. Liu, J. He, J. Lei, L. Wang, Q. Yan, *Nano Res.* **2022**, *15*, 2764.
[25] F. Shahzad, A. Iqbal, H. Kim, C. M. Koo, *Adv. Mater.* **2020**, *32*, 2002159.
[26] Y. He, Z. Deng, Y. Wang, Y. Zhao, L. Chen, *Carbohydr. Polym.* **2022**, *291*, 119572.
[27] Q. Wang, X. Pan, C. Lin, H. Gao, S. Cao, Y. Ni, X. Ma, *Chem. Eng. J.* **2020**, *401*, 126129.
[28] Y. Jiao, Y. Lu, K. Lu, Y. Yue, X. Xu, H. Xiao, J. Li, J. Han, *J. Colloid Interface Sci.* **2021**, *597*, 171.
[29] G. Ge, Y. Z. Zhang, W. Zhang, W. Yuan, J. K. El Demellawi, P. Zhang, E. Di Fabrizio, X. Dong, H. N. Alshareef, *ACS Nano* **2021**, *15*, 2698.
[30] Y. Zhu, J. Liu, T. Guo, J. J. Wang, X. Tang, V. Nicolosi, *ACS Nano* **2021**, *15*, 1465.
[31] M. Qin, W. Yuan, X. Zhang, Y. Cheng, M. Xu, Y. Wei, W. Chen, D. Huang, *Colloid. Surface. B* **2022**, *214*, 112482.
[32] Y. Lu, X. Qu, W. Zhao, Y. Ren, W. Si, W. Wang, Q. Wang, W. Huang, X. Dong, *Research* **2020**, *2020*, 2038560.
[33] W. Zhang, J. Ma, W. Zhang, P. Zhang, W. He, J. Chen, Z. Sun, *Nanoscale* **2020**, *12*, 6637.
[34] X. Li, L. He, Y. Li, M. Chao, M. Li, P. Wan, L. Zhang, *ACS Nano* **2021**, *15*, 7765.
[35] X. Wu, H. Liao, D. Ma, M. Chao, Y. Wang, X. Jia, P. Wan, L. Zhang, *J. Mater. Chem. C* **2020**, *8*, 1788.
[36] Q. Wang, X. Pan, C. Lin, X. Ma, S. Cao, Y. Ni, *Chem. Eng. J.* **2020**, *396*, 125341.
[37] J. Wei, F. Wan, P. Zhang, Z. Zeng, H. Ping, J. Xie, Z. Zou, W. Wang, H. Xie, Z. Shen, L. Lei, Z. Fu, *Chem. Eng. J.* **2021**, *424*, 130549.
[38] M. Liu, Y. Zhang, Y. Zhang, Z. Zhou, N. Qin, T. H. Tao, *Adv. Sci.* **2022**, *9*, 2102596.
[39] L. Cao, Z. Zhao, J. Li, Y. Yi, Y. Wei, *Biomacromolecules* **2022**, *23*, 1278.
[40] C. Lu, J. Qiu, W. Zhao, E. Sakai, G. Zhang, *Colloid. Surface. A* **2022**, *632*, 127793.
[41] W. Ma, W. Cao, T. Lu, Z. Jiang, R. Xiong, S. K. Samal, C. Huang, *ACS Appl. Mater. Interfaces* **2021**, *13*, 58048.
[42] H. Li, Y. Li, Q. Xu, A. Zhang, *Energy Environ. Mater.* **2020**, *3*, 192.
[43] L. Guan, H. Liu, X. Ren, T. Wang, W. Zhu, Y. Zhao, Y. Feng, C. Shen, A. V. Zvyagin, L. Fang, B. Yang, Q. Lin, *Adv. Funct. Mater.* **2022**, *32*, 2112281.
[44] L. Wang, T. Xu, X. Zhang, *TrAC, Trends Anal. Chem.* **2021**, *134*, 116130.
[45] P. Rahmani, A. Shojaei, *Adv. Colloid Interface Sci.* **2021**, *298*, 102553.
[46] S. Du, H. Suo, G. Xie, Q. Lyu, M. Mo, Z. Xie, N. Zhou, L. Zhang, J. Tao, J. Zhu, *Nano Energy* **2022**, *93*, 106906.
[47] G. Guedes, S. Wang, F. Fontana, P. Figueiredo, J. Lindén, A. Correia, R. J. B. Pinto, S. Hietala, F. L. Sousa, H. A. Santos, *Adv. Mater.* **2021**, *33*, 2007761.
[48] J. Wang, M. Shen, Z. Liu, W. Wang, *Nano Energy* **2022**, *97*, 107177.
[49] S. Zhang, B. Xu, X. Lu, L. Wang, Y. Li, N. Ma, H. Wei, X. Zhang, G. Wang, *J. Mater. Chem. C* **2020**, *8*, 6763.
[50] H. Liu, C. Du, L. Liao, H. Zhang, H. Zhou, W. Zhou, T. Ren, Z. Sun, Y. Lu, Z. Nie, F. Xu, J. Zhu, W. Huang, *Nat. Commun.* **2022**, *13*, 3420.
[51] X. Jing, H. Y. Mi, X. F. Peng, L. S. Turng, *Carbon* **2018**, *136*, 63.
[52] X. Jing, P. Feng, Z. Chen, Z. Xie, H. Li, X. F. Peng, H. Y. Mi, Y. Liu, *ACS Sustainable Chem. Eng.* **2021**, *9*, 9209.
[53] J. Mao, C. Zhao, Y. Li, D. Xiang, Z. Wang, *Etoiles Compos. Chim. Anorm. Debut Sequence Princ., Commun. Colloq. Int. Astrophys., 23rd* **2020**, *17*, 22.
[54] H. Li, H. Zheng, Y. J. Tan, S. B. Tor, K. Zhou, *ACS Appl. Mater. Interfaces* **2021**, *13*, 12814.

[55] C. Ma, Y. Wang, Z. Jiang, Z. Cao, H. Yu, G. Huang, Q. Wu, F. Ling, Z. Zhuang, H. Wang, J. Zheng, J. Wu, *Chem. Eng. J.* **2020**, *399*, 125697.
[56] Z. Wang, H. Zhou, J. Lai, B. Yan, H. Liu, X. Jin, A. Ma, G. Zhang, W. Zhao, W. Chen, *J. Mater. Chem. C* **2018**, *6*, 9200.
[57] J. Wang, T. Dai, Y. Zhou, A. Mohamed, G. Yuan, H. Jia, *J. Colloid Interface Sci.* **2022**, *613*, 94.
[58] J. Zhang, L. Wan, Y. Gao, X. Fang, T. Lu, L. Pan, F. Xuan, *Adv. Electron. Mater.* **2019**, *5*, 1900285.
[59] D. Kong, Z. M. El Bahy, H. Algadi, T. Li, S. M. El Bahy, M. A. Nassan, J. Li, A. A. Faheim, A. Li, C. Xu, M. Huang, D. Cui, H. Wei, *Adv. Compos. Hybrid Mater.* **2022**, *5*, 1976.
[60] J. Huang, X. Huang, P. Wu, *Chem. Eng. J.* **2022**, *428*, 132515.
[61] C. Wang, X. Li, E. Gao, M. Jian, K. Xia, Q. Wang, Z. Xu, T. Ren, Y. Zhang, *Adv. Mater.* **2016**, *28*, 6640.
[62] T. S. Dinh Le, J. An, Y. Huang, Q. Vo, J. Boonruangkan, T. Tran, S. W. Kim, G. Sun, Y. J. Kim, *ACS Nano* **2019**, *13*, 13293.
[63] P. Xu, X. Yao, S. Liu, H. Wang, K. Liu, A. S. Kumar, W. F. Lu, G. Bi, *Mech Mach Theory* **2021**, *161*, 104331.
[64] H. Zhang, W. Han, K. Xu, Y. Zhang, Y. Lu, Z. Nie, Y. Du, J. Zhu, W. Huang, *Nano Lett.*. **2020**, *20*, 3449.
[65] G. Wang, Q. Zhang, Q. Wang, L. Zhou, G. Gao, *ACS Appl. Mater. Interfaces* **2021**, *13*, 24173.
[66] D. Zhang, Y. Tang, Y. Zhang, F. Yang, Y. Liu, X. Wang, J. Yang, X. Gong, J. Zheng, *J. Mater. Chem. C* **2020**, *8*, 20474.
[67] H. Zhang, W. Niu, S. Zhang, *ACS Appl. Mater. Interfaces* **2019**, *11*, 24639.
[68] W. Zhao, J. Peng, W. Wang, B. Jin, T. Chen, S. Liu, Q. Zhao, W. Huang, *Small* **2019**, *15*, 1901351.